Applied Radiation and Isotopes 68 (2010) 1798–1808

Contents lists available at ScienceDirect

Applied Radiation and Isotopes

journal homepage: www.elsevier.com/locate/apradiso

Decomposition of the laboratory gamma irradiation component of angular ESR spectra of fossil tooth enamel fragments

Renaud Joannes-Boyau *, Rainer Grün, Thomas Bodin

Research School of Earth Sciences, The Australian National University, Canberra, ACT 0200, Australia

ARTICLE INFO

Article history:
Received 12 October 2009
Received in revised form
18 March 2010
Accepted 19 March 2010

Keywords:
ESR dating
Enamel fragment
CO_2^- radicals

ABSTRACT

Spectrum decomposition of the angular measurements of fossil tooth enamel fragments using an automated simulated annealing (SA) procedure shows that the mix CO_2^- radicals generated by laboratory irradiation is significantly different to that of the natural sample. The naturally irradiated sample contains about 10% of non-oriented CO_2^- radicals and a mix of 35:65 orthorhombic to axial CO_2^- radicals. In contrast, laboratory irradiation generated about 40% of non-oriented radicals and a large amount of orthorhombic CO_2^- radicals, while we failed to detect any axial CO_2^- radicals. The results indicate that geological aging of the sample incurs various annealing and transfer processes; their precise nature is yet unknown. Nevertheless, the understanding of the formation and transfer processes that leads to the observed mix of CO_2^- radicals in fossil tooth enamel is essential for the reliable application of ESR dating.

1. Introduction

This paper follows our earlier studies on the spectrum decomposition of fossil tooth enamel fragments (Joannes-Boyau et al., submitted for publication), where we introduced an automated simulated annealing (SA) procedure for the mathematical decomposition of the ESR spectra. This allowed, for the first time, to analyse all angular spectrum measurements of a tooth fragment rotated around its three major axes. The decomposition of all natural spectra required a minimum of four Gaussian lines, R_1, R_2, R_3 and B_2. All fitted components seemed to be related to anisotropic CO_2^- radicals (AICORs). R_1 was tentatively related to the g_x of orthorhombic and R_2 to $g_\perp$ of axial radicals. B_2 was regarded as a combination of g_y and $g_\parallel$ of the two AICORs. R_3 presents an envelope for misalignments, resulting from angles between the dominant axial directions and the principal axes of the fragment as well as misalignments of various crystal domains with the dominant axial direction. The ratio between R_1 and R_2 was around 35:65 and there was an angle of around 23° between the directions of R_1 and R_2.

As already pointed out by Grün et al. (2008), the natural and irradiation components in the ESR spectra of fossil teeth are distinctively different in angular measurements of tooth enamel fragments, while virtually the same for powders. They found that the natural sample had about 10% of the non-oriented CO_2^- radicals (NOCORs), while the irradiation component had around 40%. However, the irradiation component could not be fitted by a linear combination of the natural component and NOCORs, which means that there are additional differences between the natural and irradiation components of the ESR spectra (e.g. through a different distribution of orthorhombic and axial radicals). In this paper, we decompose the laboratory irradiation components of the ESR spectra (henceforth, irradiation spectra) of a tooth enamel fragment and compare the results with those from the natural sample.

2. Material and ESR measurements

The experiments were carried out on a tooth enamel fragment of a fossil bovid from the archaeological site of Holon (Porat et al., 1999). A long lamella was separated from the tooth using a dentist's diamond saw and series of consecutive fragments were cut and used for a range of heating and irradiation experiments (e.g. Grün et al., 2008; Joannes-Boyau and Grün, 2009; Joannes-Boyau et al., submitted for publication).

The methodology follows that established by Joannes-Boyau et al. (submitted for publication). *X*, *Y* and *Z* denote configurations, *x*, *y* and *z* the main axes of the measured fragment (Fig. 1), T_1, B_1 and B_2 are positions in the measured or simulated ESR spectra (see Fig. 2B), R_1, R_2, R_3 and B_2 fitted Gaussian components (Fig. 4D–G, see below). The concentrations for the radicals were derived from the double integration of the fitted lines to account for changes in the line width. For the features in the measured ESR

* Corresponding author.
E-mail address: renaud.joannes-boyau@anu.edu.au (R. Joannes-Boyau).

0969-8043/$ - see front matter © 2010 Elsevier Ltd. All rights reserved.
doi:10.1016/j.apradiso.2010.03.015

spectra, T_1–B_1 and B_2, it was not possible to carry out double integrations; their angular variations were derived from their intensities.

The fragment (H4) was successively mounted in three separate Teflon holders each containing a Parafilm mould, which allowed the incremental measurement of the fragment by rotating it around its three major axes. We used the following configurations: *X*: rotation around the axis perpendicular to the dentine–enamel junction, *Y*: around the axis of tooth growth and *Z*: perpendicular to *X* and *Y* (Fig. 1). The sample holders were inserted in a Bruker ER 218PG1 programmable goniometer and measured with a Bruker Elexys E500 ESR spectrometer in 10° increments over 360° with the following measurement conditions: 2 mW microwave power, 0.1 mT modulation amplitude 12 mT sweep width with a sweep time of 21 s. The spectra were accumulated over 50 consecutive measurements. The sample was measured before and after irradiation with a ^{137}Cs-source for 100 min, which corresponds to an approximate dose of 187 Gy.

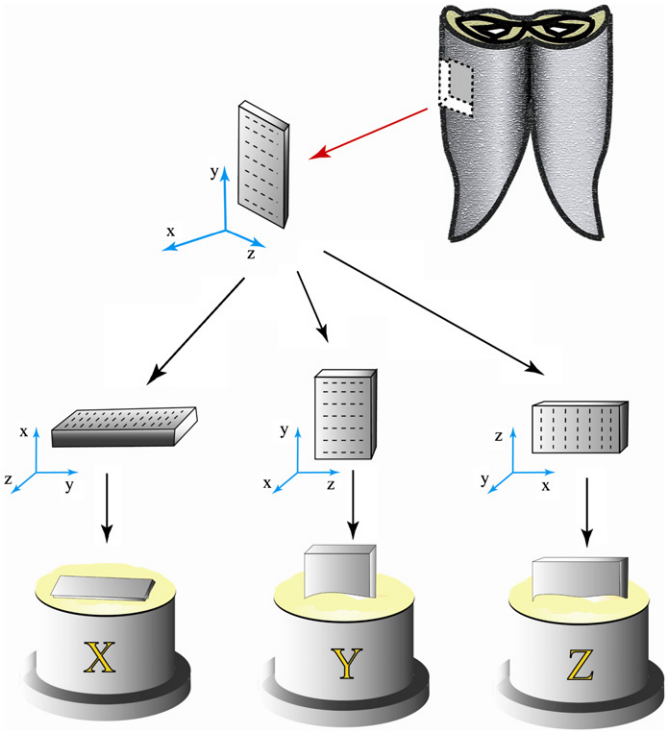

Fig. 1. Direction of axes and configurations used for the measurement of the tooth enamel fragment.

3. Spectrum decomposition

In the first step, the angular irradiation spectra were extracted by subtracting the natural spectra from the natural plus gamma irradiated. It is very important that the spectra are well aligned otherwise artefact signals are introduced. The methyl lines were used as markers for alignment (see Grün et al., 2008).

The ESR spectra of tooth enamel have a range of non-CO_2^- components, these have to be removed before decomposition. Non-radiation sensitive isotropic lines, which occur in the natural spectra (Fig. 2A), are automatically removed by the subtraction of the natural spectrum. For example, the irradiation spectra do not contain methyl lines. In addition, three wide lines were identified in the irradiation spectra, W_i1 centred at g=2.0115 with a line width (lw) of 0.3 mT, W_i2 with g=2.0081, lw=2.3 mT and W_i3 g=2.0072, lw=0.7 mT. These were combined into a single IC line and subtracted from all irradiation spectra (see Fig. 2B and C). The isotropic components of the natural spectra do not occur in the irradiation spectra, i.e. they are not radiation sensitive.

In the next step, the non-oriented CO_2^- radicals (NOCOR) were subtracted. We estimated that the remaining irradiation spectra consisted 39% of NOCORs, indicating a more than threefold increase over the natural spectra. A similar contribution was found by Grün et al. (2008). The remaining spectra are thought to contain only anisotropic components, at this stage all attributed to AICORs.

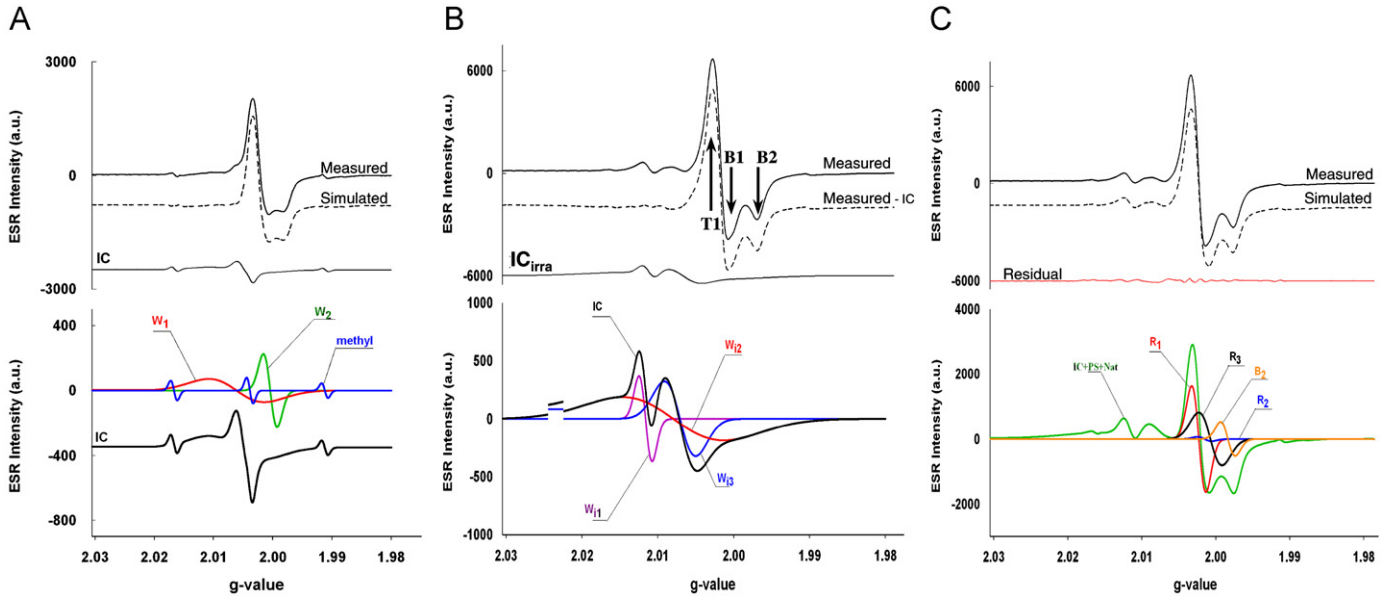

Fig. 2. Decomposition of the measured spectra. A: isotropic lines in the natural spectra (from), B: position of the isotropic lines which were combined (IC) and subtracted from all measured irradiation spectra, C: decomposition of a measured irradiation signal showing all components extracted, the natural (nat), non-oriented CO_2^- radicals (PS) and isotopic lines (IC) are combined (IC+PS+Nat), and the four main anisotropic components R_1, R_2, R_3 and B_2.

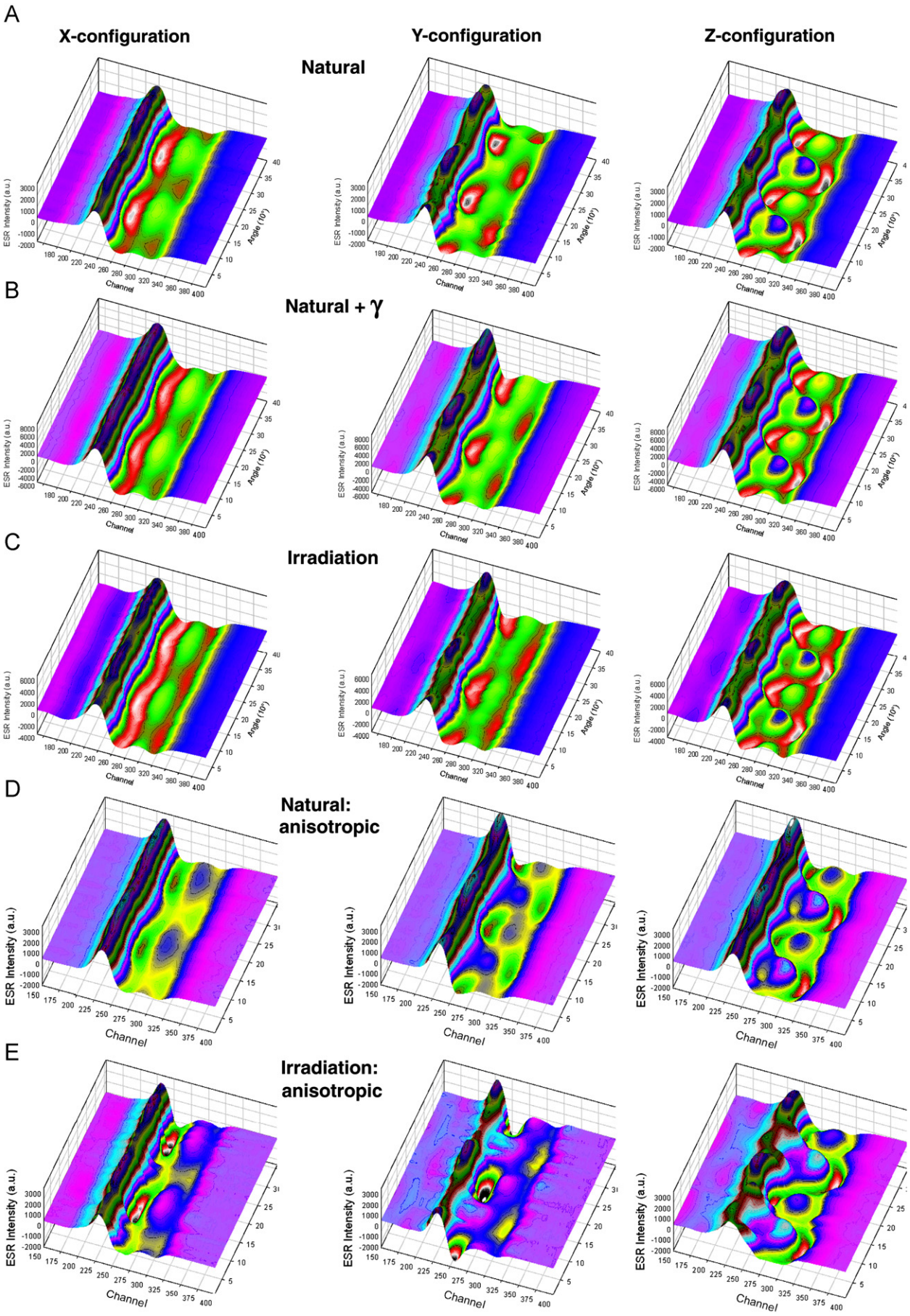

Fig. 3. Stacks of natural spectra (row A), natural plus γ (row B), irradiation (row C), natural anisotropic (row D) and irradiation anisotropic spectra (row E) for the three configurations *X*, *Y* and *Z*.

These anisotropic components of the irradiation spectra were decomposed with an automated simulated annealing (SA) procedure which is particularly well suited to separate completely overlapping signals (Joannes-Boyau et al., submitted for publication). To keep the results comparable with the previous study, the spectra were initially decomposed with four Gaussian lines, which had the same prescribed g-value range limits to avoid unrealistic solutions outside the regions for the CO_2^- radical in hydroxyapatite. No restrictions were set on the intensity, while the line widths were kept between 0.10 and 2 mT to avoid aberrations. Fig. 2C shows the composite of all subtracted components, as well as the four Gaussian lines R_1–R_3 and B_2.

4. Results and discussion

Fig. 3A and B shows the stacks of the natural and irradiated ESR spectra (natural+γ) for the different configurations. The angular variations in the measured ESR spectra (defined as the difference between maximum and minimum radical concentration or peak intensity divided by the average, $(C_{max}–C_{min})/C_{av}$)) vary from one configuration to the other. In Z-configuration (Table 1), the angular variation is significantly larger than of the other two configurations. The X-configuration shows the smallest anisotropic effects, while the Y-configuration appears to show a mixed pattern of the other two. The angular variations in the natural spectra are generally higher than in the irradiated (Table 1). The irradiation components, obtained after subtraction of the natural from the irradiated spectra, are shown in Fig. 3C. Their angular variability is also generally smaller than of the natural spectra.

Fig. 3D and E shows the natural and irradiation spectra after subtraction of the isotropic lines and NOCORs. There are striking differences between the anisotropic components of the natural and irradiation spectra. The subtraction of the NOCORs reveals that the irradiation spectra have actually much higher angular variations in T_1–B_1 than the natural spectra, but somewhat less in B_2 (see Table 1). The T_1–B_1 region is generally narrower in the irradiation spectra, particularly in the X and Y-configuration.

Fig. 4 shows the results of the fitting of the anisotropic components of the irradiation spectra in Z-configuration. The quality of the simulation is shown in the stack of the residuals (Fig. 4C). They reach a maximum of 7% in the Z-configuration and an average of 4.2%, while in Y and X the maxima are 4.7% and 5.1% and the averages 3.2% and 3.1%, respectively. These values are somewhat higher than for the natural spectra, which had maxima of 3.5%, 4.1% and 3.2% and averages of 2.9%, 3.3% and 2.8% in X, Y and Z configurations, respectively. This is not entirely surprising since extracting the irradiation spectrum includes subtracting the natural spectrum, which may create alignment problems.

The middle row in Fig. 4 shows the intensity and line-width changes for the four Gaussian components and the lower row examples of the signal intensity along with the plot of radical concentrations. The results for the decomposition of the anisotropic components of the irradiation spectra are tabulated in Table 2. For comparison, the data of the natural spectra are shown in Table 3. The lower row in Fig. 4 shows some selected fitting examples along with the angular changes in the radical concentrations. For the comparison between the natural and irradiation components, this plot is the most informative. All measurements are summarised in Fig. 5.

All fitted components show higher angular variability in the irradiation component than in the natural for all configurations. The general angular patterns for R_1, R_3 and B_2 are approximately the same in the natural and irradiation components, i.e. their maxima and minima occur at approximately the same angles. However, there is a significant change in R_2. The angular behaviour shifts by 90° in X and Y-configuration and to a 90° symmetry in Z. This is, however, the exact behaviour of R_3. This could indicate that the original component R_2 is either too small to be distinguishable from R_1 or that it does not exist at all. As pointed out before, the problem with R_3 is that it actually only approximates a Gaussian line. As a result, it would not be surprising that the prescription of an additional line could create fitting artefacts. The same does not apply to the decomposition of the natural spectra, where R_2 has an inverse behaviour to R_3 (see Fig. 5) and the region of T_1–B_1 cannot be fitted without the introduction of R_2. The X-configuration clearly shows that the radical concentration in R_3 has an effect on B_2, because angular response (or the lack thereof in X-configuration) of B_2 cannot be explained just through the angular behaviour of R_1, because B_2 would have to show an inverse concentration relationship to R_1.

To check whether R_2 can be omitted altogether, the anisotropic components of the irradiation spectra were fitted with only three components. The residuals have maximum deviations of 6.1% in the Z-configuration and 5.4% and 4.9% in Y and X, while the respective averages are 3.9%, 3.3% and 3.4%. Overall, these approximations to the measured spectra are virtually the same as for 4 Gaussian lines, which means that the introduction of an additional component had no influence on the quality of the fitting results, a first indication that R_2 does not exist as an independent component.

The results for the Z-configuration are shown in Fig. 6. While the results for R_1 are virtually unchanged, B_2 shows systematic g-value shifts (see lower row in Fig. 6). These may be the result of the pronounced 90° symmetry of R_3. Comparing the two fitting runs (Fig. 7), the angular response and radical concentrations of R_1 are virtually unchanged in all three configurations. There are some small differences in the angular behaviour of B_2 in X-configuration, but remains nearly unchanged in Y and Z. The main difference occurs for R_3 in Z-configuration, where the use of 4 Gaussian lines seemed to have split the angular behaviour into a highly anisotropic component (R_3) and less anisotropic (R_2).

In contrast to the decomposition of the natural spectra, where the use of only three Gaussian components lead to a significant and unrealistic widening of R_1 and B_2 (Joannes-Boyau et al., submitted for publication), the fitting of the irradiation spectra with three components has a negligible effect on the line widths of R_1 and B_2 (compare Tables 2 and 4).

Considering that (i) the introduction of a new component does not provide a better fit to the measured spectra, (ii) the angular behaviour of R_2 observed in the natural sample does

Table 1
Angular variations.

		T_1–B_1	B_2
Natural	Z	0.6	0.74
	Y	0.62	0.53
	X	0.31	0.4
Natural+γ	Z	0.44	0.39
	Y	0.43	0.23
	X	0.17	0.17
Natural+γ-powder-isotropic	Z	0.51	0.45
	Y	0.47	0.28
	X	0.19	0.18
Natural-powder-isotropic	Z	0.66	0.79
	Y	0.68	0.57
	X	0.33	0.43
Irradiation	Z	0.76	0.57
	Y	0.78	0.51
	X	0.45	0.46

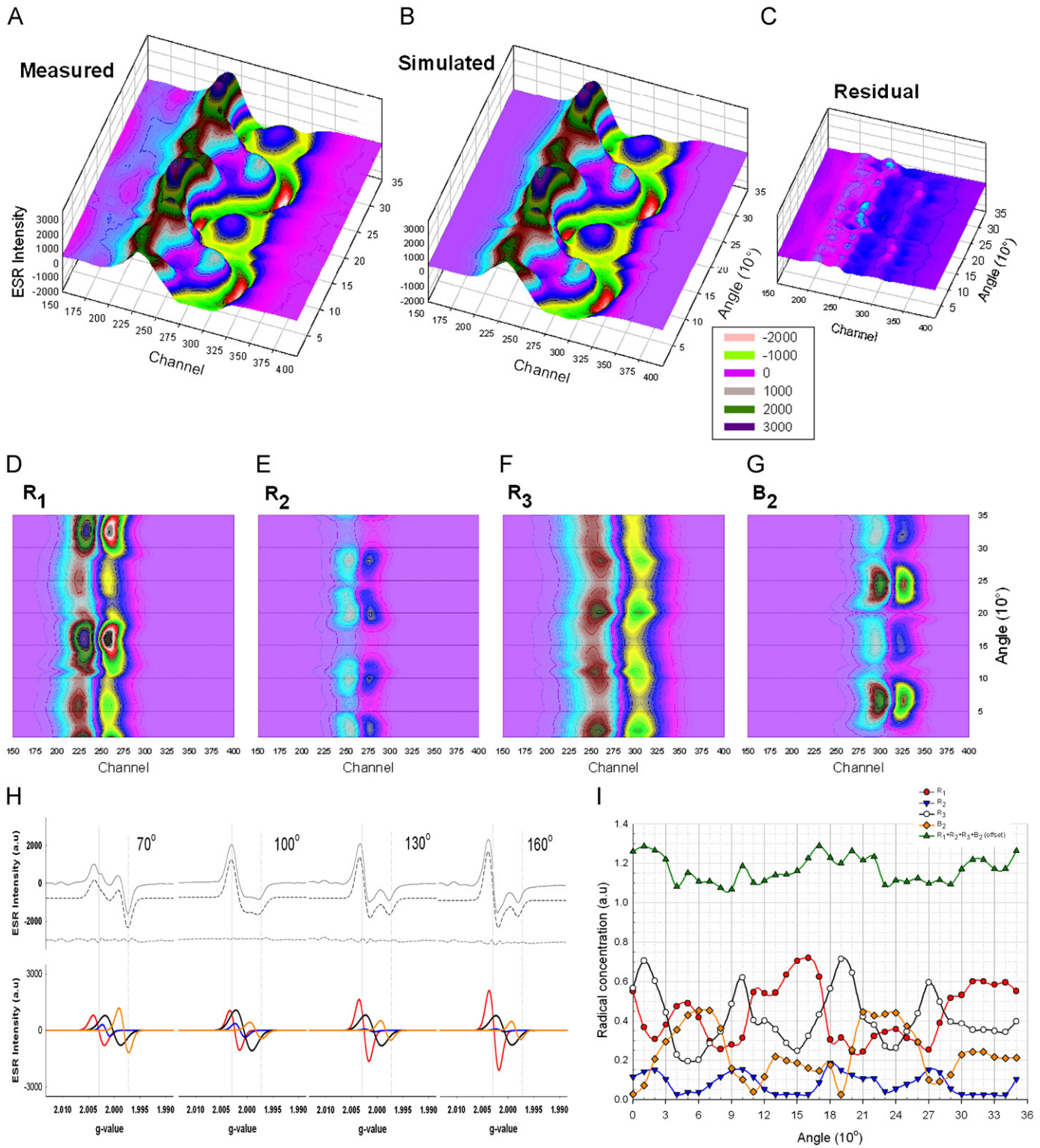

Fig. 4. Decomposition of the spectra in *Z*-configuration with four Gaussian components.A: 3D view of measured spectra., B: 3D view of simulated spectra, C: 3D view of residual (measured minus simulated), D–G: intensity maps of Gaussian components R_1, R_2, R_3 and B_2. The scale is the same as in A–C. H: decomposition of selected spectra, I: summary of all decomposition results. Note that D–H show ESR intensities, while I shows radical concentrations (obtained by double integration). These take into account changes in line width. R3 shows a 90° symmetry (arrows)).

not occur in the irradiation spectra, and (iii) the line widths of R_1 and B_2 hardly change, one can only deduce that either the natural R_2 component does not exist in the irradiation spectra at all or that it is so small that the fitting approach cannot identify it.

Joannes-Boyau et al., (submitted for publication) assessed uncertainties by running SA simulations several times on the same spectra with randomly chosen values for the initial parameters. Differences in the range 1–2% were observed for the estimation of intensities, and 4–5% for radical concentrations,

Table 2
Results of the decomposition of the anisotropic components in the irradiation spectra with four components.

	Minimum g-value angle		Maximum g-value angle		Minimum width (mT) angle		Maximum width (mT) angle		Minimum radical conc. angle		Maximum radical conc. angle		Angular variation	Average radical conc.	Relative radical conc. (%)
***Z*-configuration**															
R_1	2.0025	20	2.0029	270	0.31	0	0.41	240	0.24	80	0.72	150	0.67	0.44	37.7
R_2	2.0014	220	2.0024	250	0.26	100	0.37	0	0.02	140	0.19	180	0.87	0.08	7.0
R_3	2.0002	280	2.0010	10	0.51	110	0.54	20	0.20	50	0.71	190	0.72	0.41	35.1
B_2	1.9980	270	1.9988	150	0.29	190	0.45	40	0.02	110	0.45	210	0.95	0.24	20.2
***Y*-configuration**															
R_1	2.0025	260	2.0029	0	0.26	310	0.32	150	0.15	80	0.70	180	0.78	0.42	43.0
R_2	2.0012	220	2.0016	20	0.26	130	0.41	180	0.03	170	0.20	40	0.85	0.12	12.3
R_3	2.0002	0	2.0008	180	0.35	160	0.46	130	0.15	180	0.47	100	0.68	0.28	28.3
B_2	1.9985	260	1.9989	120	0.26	250	0.37	130	0.10	180	0.32	270	0.69	0.16	16.4
***X*-configuration**															
R_1	2.0026	150	2.0029	30	0.26	30	0.32	250	0.19	210	0.71	300	0.73	0.45	43.8
R_2	2.0016	40	2.0019	130	0.27	50	0.36	330	0.00	130	0.17	20	1.00	0.08	7.8
R_3	2.0012	50	2.0012	70	0.48	90	0.54	140	0.14	110	0.66	40	0.79	0.40	39.2
B_2	1.9984	320	1.9988	60	0.28	0	0.37	90	0.07	10	0.20	170	0.66	0.09	9.2

Table 3
Results of the decomposition of the anisotropic components in the natural spectra (from Joannes-Boyau et al. submitted for publication).

	Minimum g-value angle		Maximum g-value angle		Minimum width (mT) angle		Maximum width (mT) angle		Minimum radical conc. angle		Maximum radical conc. angle		Angular variation	Average radical conc.	Average radical conc.
***Z*-configuration**															
R_1	2.0025	190	2.0027	210	0.28	330	0.35	110	0.28	110	0.5	330	0.58	0.38	17.7
R_2	2.002	280	2.0024	60	0.36	190	0.42	300	0.5	50	0.65	180	0.26	0.58	27.0
R_3	2.0003	80	2.0006	160	0.39	90	0.47	180	0.51	150	0.82	170	0.47	0.65	30.2
B_2	1.9982	230	1.9987	10	0.33	230	0.42	0	0.43	350	0.65	80	0.41	0.54	25.1
***Y*-configuration**															
R_1	2.0026	80	2.0028	350	0.27	170	0.32	280	0.22	80	0.48	0	0.54	0.36	18.2
R_2	2.0019	110	2.0023	350	0.38	110	0.42	320	0.42	60	0.66	170	0.41	0.57	28.8
R_3	2.0004	270	2.0006	110	0.41	130	0.48	310	0.56	20	0.74	280	0.28	0.65	32.8
B_2	1.9985	320	1.9988	100	0.36	70	0.42	300	0.3	340	0.52	80	0.54	0.4	20.2
***X*-configuration**															
R_1	2.0026	20	2.0028	150	0.27	150	0.31	260	0.22	210	0.39	120	0.43	0.29	14.9
R_2	2.002	20	2.0023	290	0.41	110	0.42	280	0.6	210	0.72	290	0.18	0.67	34.5
R_3	2.0003	110	2.0006	200	0.47	130	0.54	300	0.62	120	0.77	210	0.22	0.69	35.6
B_2	1.9984	130	1.9987	220	0.39	70	0.42	300	0.19	140	0.38	330	0.49	0.29	14.9

keeping in mind that the latter is the product of intensity and line width squared. For a second assessment of the uncertainties in the simulation, the decomposition was carried out on the irradiated spectra that had only the NOCORs and the isotropic lines subtracted (i.e. natural plus gamma minus isotropic lines). This allows the comparison of the behaviour of Gaussian components from the decomposition of the (natural+irradiated) spectra with the combined, separate results of the natural and irradiation components (Fig. 8). Normalising on the combined averages of the components, deviations between 3.4% and 8.5% are observed. Using three Gaussian components, a somewhat better agreement is achieved for R_1 (6.1%) and B_2 (6.2%). The latter is probably caused by the observed *g*-value changes in the fitting of the irradiation spectra (see Fig. 6F). However, the major features, such as the angles of the maxima and minima, or the symmetry (180° versus 90°) remain unchanged.

Our decompositions show that there is a profound difference between the natural and irradiation spectra in fossil tooth enamel:

- the natural spectra contain a 9% component of NOCORs, the irradiation spectra 39%;
- the methyl line and other isotropic lines which occur in the natural spectra are not irradiation sensitive;
- the irradiation spectra contain three additional wide lines;
- the angular variation of all fitted components is significantly higher in the irradiation spectra than the natural;
- the natural spectra have a R_1:R_2 ratio of 35:65, the irradiation spectra do not contain an identifiable component that shows an angular behaviour as R_2 in the natural spectra.

The observations on the various isotropic lines have been reported by many authors. The occurrence of two different AICORs in fossil tooth enamel was described in the two previous studies of Joannes-Boyau and Grün (2009) and Joannes-Boyau et al., (submitted for publication) and is supported by Q-band studies on fossil enamel fragments (Bouchez et al., 1988, Rossi and Poupeau, 1990). The Q-band experiments also demonstrated that axial and orthorhombic CO_2^- radicals had different orientations and that the orthorhombic radical was less stable than the axial. Vorona et al. (2006) suggested that in modern teeth orthorhombic radicals could convert into axial by heating.

The higher angular variations of the irradiation spectrum are most probably the result that only one anisotropic radical is

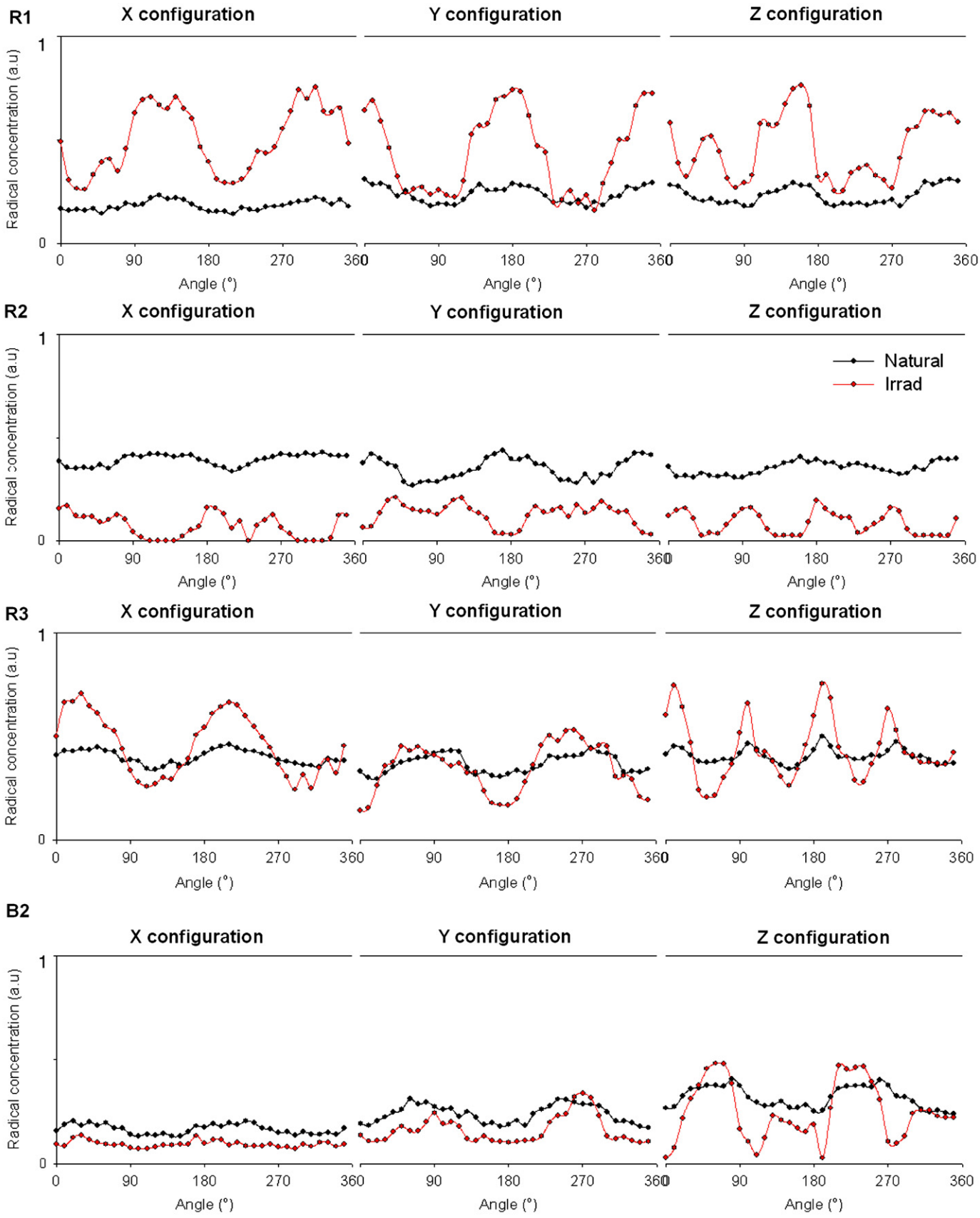

Fig. 5. Summary of the angular behaviour of the anisotropic components of the natural spectra as well as the irradiation spectra decomposed with four Gaussian components.

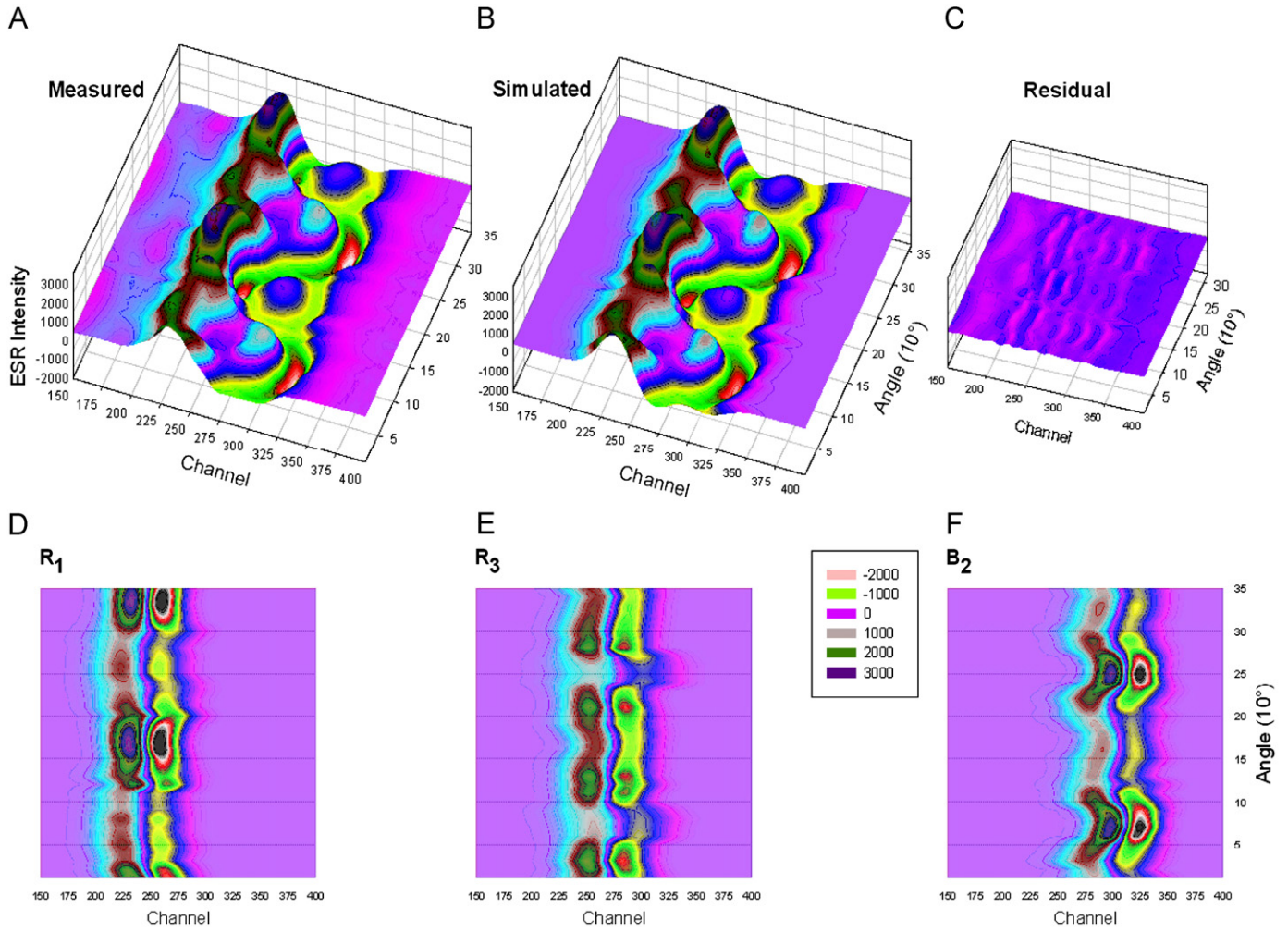

Fig. 6. Decomposition of the spectra in *Z*-configuration with three Gaussian components. A: 3D view of measured spectra., B: 3D view of simulated spectra, C: 3D view of residual (measured minus simulated), D–F: intensity maps of Gaussian components R_1, R_3 and B_2. The scale is the same as in A–C).

present. The overlapping of two radicals in the same region, particularly when having somewhat different orientation will always lead to a muting of angular response. The observed increase in angular variability after heating was tentatively attributed by Joannes-Boyau and Grün (2009) to a higher crystalinity. It seems, however, that rather than changing the crystal properties, heating reduces the mix of different CO_2^- radicals, as a consequence leading to higher angular variabilities.

It is reasonable to assume that low dose rate natural radiation generates a similar mix of radicals as high dose rate laboratory irradiation. However, the geological aging of the sample incurs various annealing and transfer processes. Clearly, a large proportion of the NOCORs disappear, while virtually all R_2 (axial) components appear. At this stage, it is not possible to speculate whether NOCORs, R_1 radicals, or both lead to the formation of R_2 over time. It is also not clear whether there are transfers between the isotropic components and the various CO_2^- radicals. The understanding of the formation and transfer processes that lead to the observed mix of the CO_2^- radicals in fossil tooth enamel is essential for the reliable application of ESR dating.

If the kinetics of the decay of orthorhombic CO_2^- radicals and formation of the axial were known, their ratio could be used for rough age assessments. While this will not approximate the precision of conventional ESR dating, it may be helpful in cases their dose rate assessments are impossible, e.g. when working on archaeological collections.

R_3 is a problematic component and its nature remains unclear. R_3 is needed for minimising the angular dependency of the sum of all fitted components. The behaviour of B_2 indicates that R_3 is a component related to the AICORs (see Fig. 5, *X*-configuration). Keeping in mind that enamel fragments are partially ordered systems with some preferential direction of the hydroxyapatite crystals, R_3 can be designated as a heterogeneous signal composed by misalignments of R_1 in the irradiation spectra and R_1 and R_2 in the natural. R_3 would then consist of a semi-infinite series (in the case of discrete values (1.1)) of Gaussian components with varying amplitudes between the T_1 and B_2 positions and can be described by

$$f(\chi) = \sum_{a}^{b} A(\mu) \left(\frac{\mu-\chi}{\sigma^3}\right) e^{\left(\frac{-(\mu-\chi)^2}{2\sigma^2}\right)} d\mu, \tag{1.1}$$

with a and b the positions of T_1 and B_2, μ and σ are the centre and the width of each Gaussian lines, respectively. $A(\mu)$ is the amplitude function of each integrated Gaussian lines.

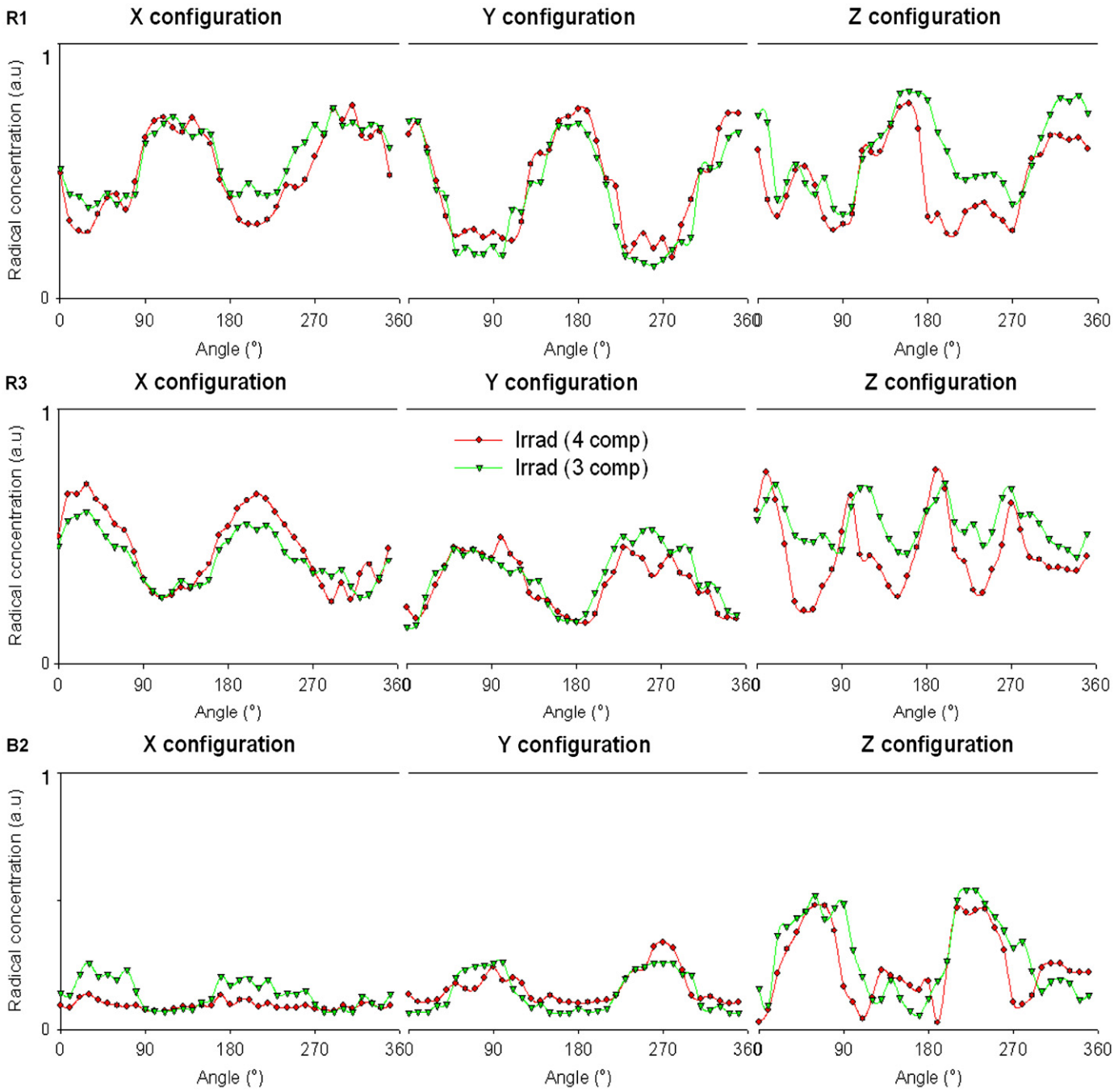

Fig. 7. Summary of the angular behaviour of the anisotropic components of the natural spectra as well as the irradiation spectra decomposed with three Gaussian components.

Both χ and μ are independent spatial variables on the g-value axis. Eq. (1.1) gives the intensity of R_3 at any χ value that the variable can take along the g-value axis. For a given χ, $f(\chi)$ is the sum of all the values taken by Gaussian functions (with different μ centres) at this specific χ position. A part of this equation is known as the error function (erf). This erf function has an influence on the line shape. For example, if $A(\mu)$ is a linear function, $f(\chi)$ may be approximated by a Gaussian function if the magnetic field is located between T_1 and B_2. In future simulations, we will endeavor to add this function to our simulation program.

5. Conclusions

This study shows that the radiation response of fossil tooth enamel is significantly more complicated than previously thought. Apart from a very high proportion of AICORs, the irradiation spectra do not contain any identifiable axial CO_2^- component, which, on the other hand, dominates the natural spectra. Keeping in mind that various ESR dating attempts have been accompanied with some degree of success, it seems that most of the radicals are converted from one type to another without much reducing the overall radical concentration. To enhance our understanding of potential

Table 4
Results of the decomposition of the anisotropic components in the irradiated spectra with three components.

	Minimum g-value angle		Maximum g-value angle		Minimum width (mT) angle		Maximum width (mT) angle		Minimum radical conc. angle		Maximum radical conc. angle		Angular variation	Average radical conc.	Relative radical conc. (%)
***Z*-configuration**															
R_1	2.0023	210	2.0031	120	0.32	340	0.44	240	0.37	110	0.90	180	0.95	0.65	36.1
R_3	2.0005	260	2.0013	40	0.37	0	0.54	250	0.47	0	0.79	220	0.52	0.62	34.3
B_2	1.9982	270	1.9990	40	0.30	260	0.44	210	0.27	190	0.82	240	0.67	0.53	29.6
***Y*-configuration**															
R_1	2.0028	260	2.0031	160	0.28	250	0.33	170	0.15	340	0.78	80	1.43	0.45	44.8
R_3	2.0009	150	2.0015	20	0.37	140	0.50	250	0.16	80	0.59	330	1.12	0.39	38.9
B_2	1.9988	260	1.9990	150	0.28	90	0.36	20	0.07	70	0.29	170	0.76	0.16	16.3
***X*-configuration**															
R_1	2.0027	90	2.0030	330	0.28	300	0.34	220	0.41	50	0.84	310	0.70	0.61	49.9
R_3	2.0011	250	2.0016	150	0.37	150	0.54	60	0.29	150	0.67	70	0.82	0.46	37.6
B_2	1.9986	50	1.9989	160	0.28	160	0.41	90	0.08	70	0.29	170	0.74	0.15	12.6

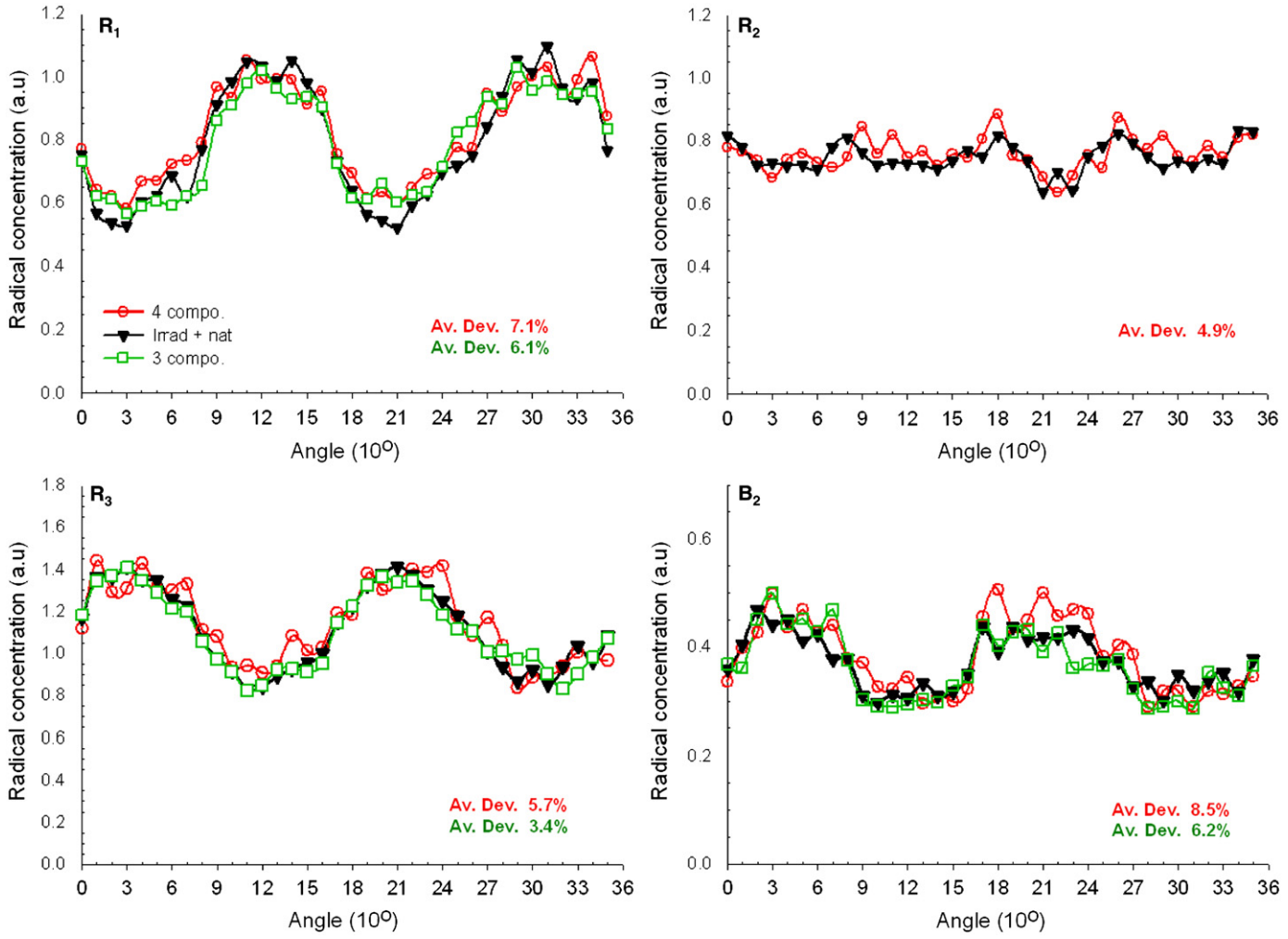

Fig. 8. Comparison of angular components from the decomposition of the natural+irradiation spectra and the sum of the separate decompositions of natural and irradiation spectra.

transfer processes occurring between radicals, an upcoming kinetics study appears critically required now.

Acknowledgments

We thank N. Manson, Research School of Physical Sciences, ANU, for helpful comments. We are grateful to F. Callens and Henk Vrielinck, Gent, for their thorough advice in the earlier stages of this study. RG is grateful to the Institut des Sciences humaines et sociales du CNRS, Bordeaux, and the Laboratoire d'Anthropologie des populations du Passé, Université de Bordeaux I, for their kind hospitality in the writing-up stage of this manuscript. Aspects of this study were supported by ARC DP0664144 *Microanalysis of human fossils: new insights into age, diet and migration*.

References

Bouchez, R., Cox, R., Hervé, A., Lopez-Carranza, E., Ma, J.L., Piboule, M., Poupeau, G., Rey, P., 1988. Q-Band ESR studies of fossil teeth: consequences for ESR dating. Quaternary Science Reviews 7, 497–501.

Grün, R., Joannes-Boyau, R., Stringer, C., 2008. Two types of CO_2^- radicals threaten the fundamentals of ESR dating of tooth enamel. Quaternary Geochronology 3, 150–172.

Joannes-Boyau, R., Grün, R., 2009. Thermal behavior of oriented and non-oriented CO_2^- radicals in tooth enamel. Radiation Measurments 44, 505–511.

Joannes-Boyau, R., Bodin, T., Grün, R. submitted for publication. Decomposition of the angular ESR spectra of fossil tooth enamel fragments. Radiation Measurements.

Porat, N., Zhou, L.P., Chazan, M., Noy, T., Horwitz, L.K., 1999. Dating the lower paleolithic open-air site of Holon, Israel by luminescence and ESR technologies. Quaternary Research 51, 328–341.

Rossi, A.M., Poupeau, G., 1990. Radiation damage in bioapatites: the ESR spectrum of irradiated enamel revisited. Radiation Measurements 17, 537–545.

Vorona, I.P., Ishchenko, S.S., Baran, N.P., Petrenko, T.L., Rudko, V.V., 2006. Evidence of annealing-induced transformation of CO_2^- radicals in irradiated tooth enamel. Radiation Measurements 41, 577–581.